AFRL-RX-WP-TP-2008-4342

NOMINAL VERSUS LOCAL SHOT-PEENING EFFECTS ON FATIGUE LIFETIME IN Ti-6Al-2Sn-4Zr-6Mo AT ELEVATED TEMPERATURE (Preprint)

S.K. Jha, R. John, and J.M. Larsen

Behavior/Life Prediction Section
Metals Branch

SEPTEMBER 2008
Interim Report

Approved for public release; distribution unlimited.

See additional restrictions described on inside pages

STINFO COPY

AIR FORCE RESEARCH LABORATORY
MATERIALS AND MANUFACTURING DIRECTORATE
WRIGHT-PATTERSON AIR FORCE BASE, OH 45433-7750
AIR FORCE MATERIEL COMMAND
UNITED STATES AIR FORCE

REPORT DOCUMENTATION PAGE

Form Approved
OMB No. 0704-0188

The public reporting burden for this collection of information is estimated to average 1 hour per response, including the time for reviewing instructions, searching existing data sources, searching existing data sources, gathering and maintaining the data needed, and completing and reviewing the collection of information. Send comments regarding this burden estimate or any other aspect of this collection of information, including suggestions for reducing this burden, to Department of Defense, Washington Headquarters Services, Directorate for Information Operations and Reports (0704-0188), 1215 Jefferson Davis Highway, Suite 1204, Arlington, VA 22202-4302. Respondents should be aware that notwithstanding any other provision of law, no person shall be subject to any penalty for failing to comply with a collection of information if it does not display a currently valid OMB control number. **PLEASE DO NOT RETURN YOUR FORM TO THE ABOVE ADDRESS**.

1. REPORT DATE ***(DD-MM-YY)***
September 2008

2. REPORT TYPE
Journal Article Preprint

3. DATES COVERED ***(From - To)***

4. TITLE AND SUBTITLE
NOMINAL VERSUS LOCAL SHOT-PEENING EFFECTS ON FATIGUE LIFETIME IN Ti-6Al-2Sn-4Zr-6Mo AT ELEVATED TEMPERATURE (Preprint)

5a. CONTRACT NUMBER
IN HOUSE

5b. GRANT NUMBER

5c. PROGRAM ELEMENT NUMBER
62102F

5d. PROJECT NUMBER
4347

5e. TASK NUMBER
RG

5f. WORK UNIT NUMBER
M02R3000

6. AUTHOR(S)
S.K. Jha, R. John, and J.M. Larsen

7. PERFORMING ORGANIZATION NAME(S) AND ADDRESS(ES)
Behavior/Life Prediction Section
Metals Branch
Metals, Ceramics, and NDE Division
Materials and Manufacturing Directorate
Wright-Patterson Air Force Base, OH 45433-7750

8. PERFORMING ORGANIZATION REPORT NUMBER
AFRL-RX-WP-TP-2008-4342

9. SPONSORING/MONITORING AGENCY NAME(S) AND ADDRESS(ES)
Air Force Research Laboratory
Materials and Manufacturing Directorate
Wright-Patterson Air Force Base, OH 45433-7750
Air Force Materiel Command
United States Air Force

10. SPONSORING/MONITORING AGENCY ACRONYM(S)
AFRL/RXLMN

11. SPONSORING/MONITORING AGENCY REPORT NUMBER(S)
AFRL-RX-WP-TP-2008-4342

12. DISTRIBUTION/AVAILABILITY STATEMENT
Approved for public release; distribution unlimited.

13. SUPPLEMENTARY NOTES
PAO case number 88ABW-2008-0104, cleared 09 September 2008. This is a work of the U.S. Government and is not subject to copyright protection in the United States. Paper contains color.

14. ABSTRACT
A study of the elevated temperature fatigue lifetime variability in the shot-peened condition of the a+b titanium alloy, -Ti-6Al-2Sn-4Zr-6Mo, is presented. It is shown that failures separate into two distributions: (i) governed by the nominal residual stress profile, promoting subsurface crack initiation and longer lifetimes, and (ii) the life-limiting behavior that is controlled by localized material-shot-peening interaction. In the residual-stress-free condition, failures occurred predominantly by surface crack initiation at the microstructural scale, on the order of 10 um, by crystallographic facet formation in one of a few a particles and/or colonies. This mechanism was mitigated under the nominal shot-peening residual stress profile, producing failures initiating from the subsurface region by crystallographic faceting spread over a significantly larger area (equivalent diameter of about 100-200 um) thank in the absence of residual stress.

15. SUBJECT TERMS
Fatigue variability, lifetime distribution, shot-peening, residual stress, Ti-6Al-2Sn-4Zr-6Mo

16. SECURITY CLASSIFICATION OF:			**17. LIMITATION OF ABSTRACT:**	**18. NUMBER OF PAGES**	**19a. NAME OF RESPONSIBLE PERSON** (Monitor)
a. REPORT	**b. ABSTRACT**	**c. THIS PAGE**			James M. Larsen
Unclassified	Unclassified	Unclassified	SAR	30	**19b. TELEPHONE NUMBER** *(Include Area Code)* (937) 255-9791

Nominal versus Local Shot-Peening Effects on Fatigue Lifetime in Ti-6Al-2Sn-4Zr-6Mo at Elevated Temperature

S. K. Jha[*], R. John, and J. M. Larsen

US Air Force Research Laboratory, AFRL/RXLMN, Materials and Manufacturing Directorate, Wright-Patterson AFB, OH 45433, USA
[*]Universal Technology Corporation, Dayton, OH 45432, USA

Abstract

A study of the elevated temperature (260°C) fatigue lifetime variability in the shot-peened condition of the α+β titanium alloy, Ti-6Al-2Sn-4Zr-6Mo, is presented. It is shown that failures separate into two distributions: (i) governed by the nominal residual stress profile, promoting subsurface crack initiation and longer lifetimes, and (ii) the life-limiting behavior that is controlled by localized material – shot-peening interaction. In the residual-stress-free condition, failures occurred predominantly by surface crack initiation at the microstructural scale, on the order of 10 μm, by crystallographic facet formation in one or a few α particles and/or colonies. This mechanism was mitigated under the nominal shot-peening residual stress profile, producing failures initiating from the subsurface region by crystallographic faceting spread over a significantly larger area (equivalent diameter of about 100-200 μm) than in the absence of residual stress. Although the microstructure-scale surface crack-initiation was suppressed, the life-limiting failures under shot-peening continued to occur by surface initiation but through an apparently larger crack initiation size by formation of a flat, non-crystallographic fracture area (equivalent diameter of about 60-200 μm) at the crack origin.

Keywords: Fatigue variability, lifetime distribution, shot-peening, residual stress, Ti-6Al-2Sn-4Zr-6Mo

1. INTRODUCTION

The compressive-residual-stress-producing treatments, including shot-peening (SP), have been shown to enhance the resistance of a surface to fatigue crack initiation and propagation [1-5]. Often, the benefit to lifetime is measured in terms of the mean-fatigue behavior, which exhibits significant improvement upon SP due to, depending on the loading conditions, shift in the failure initiation from surface to the subsurface regions [6-8] or delayed crack initiation and/or retardation of crack growth from the surface [9-12]. The driving force for crack initiation is thought to be reduced due to the uniform distribution of immobile dislocations in the peened surface layer, which restricts the motion of dislocations and development of intense slip bands during fatigue loading [13, 14]. Along similar lines, others have attributed the delay in crack initiation to a decreased level of plastic strain accumulation in the work-hardened surface material [4, 14]. The retardation of crack propagation or crack arrest is related to the significant reduction in the effective stress intensity factor range under the compressive residual stress (RS) profile [9, 10, 15, 16] as well as the decreased crack-tip plasticity due to work hardening [17].

It is also well documented that the degree of influence on the lifetime is strongly dependent on the stress level and temperature regime [7, 8, 11, 18, 19] as well as the stress gradient [9]. In particular, the subject of residual stress (RS) relaxation has been given a widespread attention [7, 9, 20-22] in this regard. At cyclic stress levels above the material yield strength, under the global-yield condition, and/or at high temperatures, the benefit of SP could decrease due to relaxation of the RS profile [7, 14, 23, 24]. At lower stress levels, i.e., the long-lifetime regime, the SP effect may be reduced if failure would have predominantly occurred by subsurface crack initiation in an otherwise RS-free condition [18] or due to the dominance of crack initiation in the total lifetime [4]. The latter being a more influential factor in notch fatigue [2, 23] than

smooth fatigue. The SP-induced surface roughness, which has also been given an important consideration in several studies [7, 8, 26], can have a competing influence on the positive effects of the compressive stress and the cold work level, especially under thermal-mechanical conditions where the RS profile may significantly relax.

It is clear, that the response of a SP-induced (or any other treatment) RS profile to the variables encountered in service and the effect on lifetime has to be completely understood in order to accurately incorporate it in life prediction. Several lifing approaches incorporating these mechanisms have been proposed [4, 9, 10, 15] where the fatigue lifetime behavior with respect to the global RS and cold work levels have been predicted. In addition, another pervasive consideration in life-prediction is the role of surface treatment in the lifetime distribution rather than the mean-lifetime effects. However, this aspect has not been sufficiently addressed in past SP studies. In the RS-free condition, for instance, it has been demonstrated that the average microstructure or the distribution about the mean characteristics is not an accurate predictor of the lifetime variability [27, 28]. In particular, the lower-tail of lifetime has been shown to be often controlled by an extreme microstructural configuration or arrangement, which otherwise has a small probability of occurrence, and may not be accounted for in conventional statistical characterization of microstructure [29]. In aerospace applications, many parts are surface-treated and it is important to determine if in that condition the life-limiting behavior can be accurately extrapolated from the nominal fatigue behavior deduced from the characterization of the RS profile.

In light of the above, the objective of this paper is to analyze the distribution in lifetime under a relevant SP condition, at a given stress level and temperature in the turbine engine alloy, Ti-6Al-2Sn-4Zr-6Mo (Ti-6-2-4-6). The experimental conditions were chosen to target a regime

where failure is invariably by surface crack-initiation in the absence of surface treatment, and also to avoid a regime where the RS may significantly relax. It is shown that lifetime variability separates into two behaviors; one driven by the nominal RS-level, and second, a life-limiting behavior controlled by the local, material-SP interaction effects. This, nominal vs. life-limiting approach to measuring the benefit of a surface treatment can be of key significance in accurately incorporating the RS in probabilistic life-prediction.

2. MATERIAL AND EXPERIMENTAL PROCEDURE

2.1 Material

The material in this study was the $\alpha+\beta$ titanium alloy, Ti-6-2-4-6, in the duplex microstructural condition. Two variants of the microstructure, which differed moderately in terms of optical characterization, were considered. These were designated as microstructures A and B, and are presented in Fig. 1 (a) and (b) respectively. As shown, microstructure B had a higher volume fraction of primary equiaxed-α particles, about 33%. Microstructure A had approximately 19% volume fraction of primary α. Second, microstructure B displayed a relatively smaller aspect-ratio of secondary, lath-α. These microstructures also varied in terms of their crystallographic texture as reported elsewhere [27]. Besides these characteristics, both microstructures consisted of microtextured regions [30] and preliminary study indicated that they differed in terms of the size and degree of microtexturing.

The tensile behavior, at 260°C, of the two microstructures was nominally similar as depicted by Fig 2. The 0.2% yield strengths were about 850 and 825 MPa and the ultimate tensile strengths were about 1040 and 1012 MPa respectively of microstructures A and B (Fig. 2).

2.2 Experimental Procedure

The fatigue specimens were electro-discharge machined in the circumferential orientation from forgings of the two microstructures. The final machining was done by low stress grinding (LSG). The round-bar geometry with the gage-diameter of about 4 mm and the gage-length of about 12.5 mm was employed. In order to produce a residual-stress-free surface, the specimens were electropolished to remove about 50 μm layer from the surface. For the samples used in the RS study, peening was performed on the LSG surface.

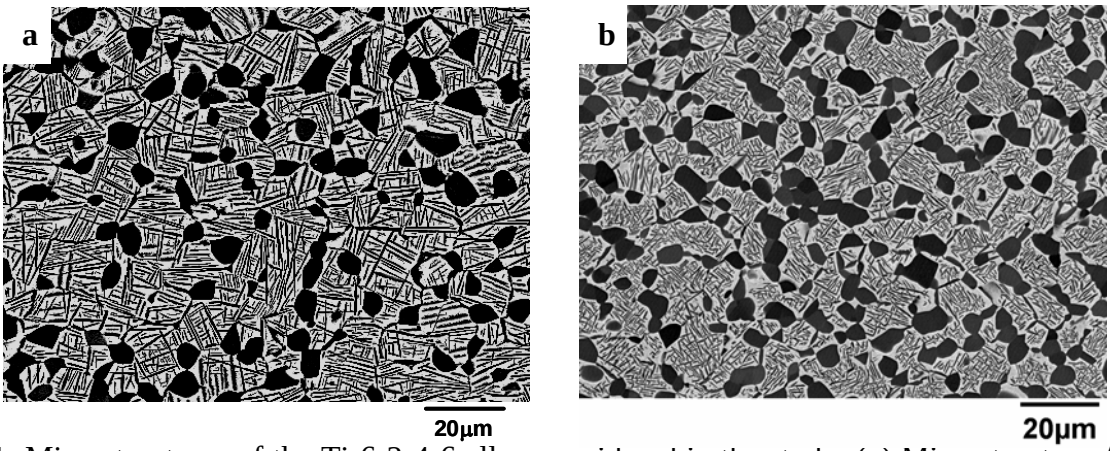

Fig. 1: Microstructures of the Ti-6-2-4-6 alloy considered in the study; (a) Microstructure A and (b) Microstructure B

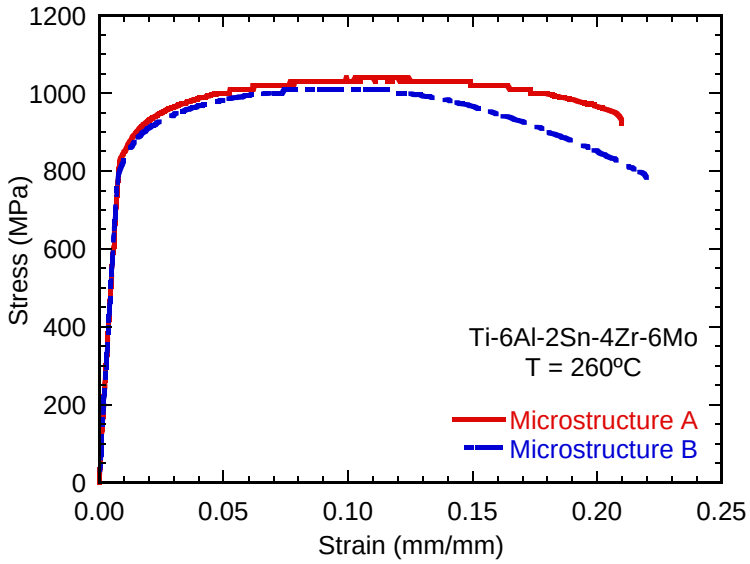

Fig. 2: Tensile behavior of Ti-6-2-4-6 microstructures at 260°C

The fatigue experiments were conducted in an automated servohydraulic test system. Axial, load-controlled fatigue, at the frequency of 20 Hz, and the stress ratio (R) of 0.05 was employed. A constant amplitude sine-wave profile was applied with the maximum stress of 860 MPa. The test temperature was 260°C and the atmosphere was lab air.

Elevated temperature experiments were accomplished in two types of test configurations: (i) a resistance heating furnace using a button-head type gripping assembly, and (ii) a four-zone quartz-lamp heating system with collet grips. In (i), two thermocouples were welded at the gage ends of the specimen for temperature control. In (ii), four loop-thermocouples were mounted along the gage length that independently controlled the temperature in each zone. Additionally, two thermocouples were welded in the upper and lower shoulder regions of the specimen, which were maintained at the test temperature with the help of resistance coils. The quartz-lamp system was employed in all experiments involving SP. The heating rate and the soaking time at temperature before commencing a test were kept constant across all tests to minimize any variation in the thermal relaxation of RS between specimens prior to cycling.

The microstructural characterization was done in a field emission Scanning Electron Microscopes (SEM) in the back-scattered electron mode. The same SEMs were also used in the fracture surface analysis. The crack initiation area was determined from the convergence of the radial crack-growth marks. The crack initiation area was outlined and measured using the ImagePro image analysis program. The spatial angles of crack initiation facets were measured by quantitative tilt fractography with the aid of the MeX image analysis program. This required the input of stereo-image pairs (at 0 and 6° tilts) of the crack initiation region at a fixed working distance, which were acquired in the SEM.

3. SURFACE TREATMENT, RESIDUAL STRESS, AND RELAXATION

SP produces the compressive RS by plastically deforming the surface layer, which is accomplished by impacting the work-piece with a hard medium (or shots) [1]. The SP process variables need to be closely controlled to obtain the targeted RS profile as well as a uniform surface condition. The peening configuration in the present study is schematically illustrated in Fig. 3 where the relative dimensions of the specimen and the shots have been drawn to scale. For the purpose of this study, typical SP parameters applicable to titanium surfaces were invoked. In this, spherical steel beads of 0.5 mm diameter were used as the impacting medium. The peening intensity was 6A-0+2A (Almen A scale per the ASME specification) and the coverage was 100%. Each sample was subjected to an inspection by a fluorescent tracer coating method to ensure that the coverage was complete. The peening was done on the previously LSG surface, which ensured uniformity of surface between specimens prior to peening. In order to minimize any process variability, specimens from the two microstructures were randomized and peened in a single batch.

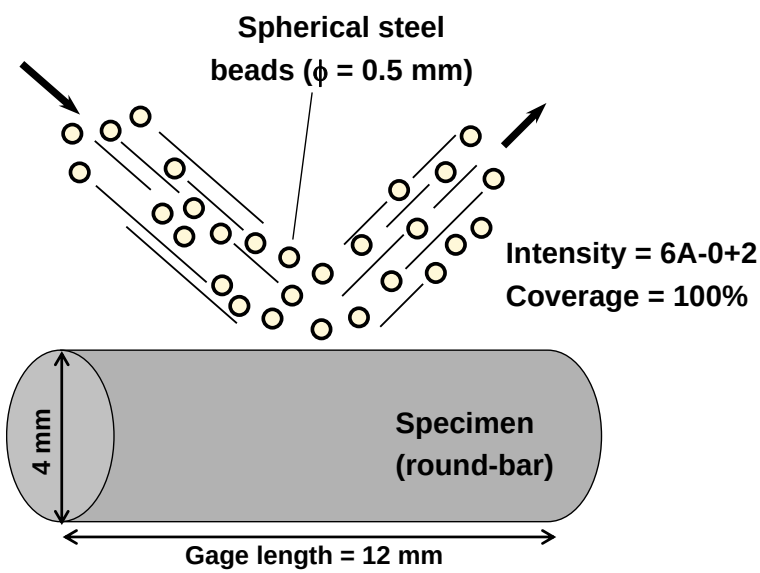

Fig. 3: Schematic of the peening configuration in the present study. The relative dimensions of shots and specimen are drawn to scale.

The baseline RS profile produced by the SP treatment is presented in Fig. 3. The RS levels were measured by the X-ray diffraction technique [31] via destructive layer removal. The figure depicts that a compressive RS of about 860 MPa was produced at the surface with the maximum reaching about 1000 MPa just below the surface (~ 20 μm). The depth of the compressive layer was about 160 μm. It is well known that the RS field relaxes upon fatigue and/or with exposure to elevated temperature [7, 12, 20-22]. The relative contributions of the two primary components of the relaxation process, mechanical and thermal, are strongly dependent on the initial RS profile, the temperature, and the applied load level [7, 21, 22]. In general, the mechanical relaxation is attributed to stress redistribution over the specimen cross-section due to cyclic softening of the material [22]. The thermal relaxation of RS has been related to the healing of crystalline defects, which are produced during SP, by thermally-activated processes [15, 21]. A detailed discussion of these relaxation effects in Ti-6-2-4-6 will be the subject of another paper [24]. Here, the relaxed RS profile was measured upon completion of a fatigue test (presumably containing contributions from both factors) and is shown in Fig. 4 [24]. The measurements were made in the gage section of samples with failure lifetime in the range of 97,337 to 350,984 cycles. The relaxed profiles shown in the figure represent the measurements from 7 samples (6 of microstructure A and 1 of microstructure B). A moderate degree of relaxation, especially in the near surface regions, is clearly evident here (Fig. 3) although there was a considerable degree of variability between profiles. However, the figure also clearly demonstrates that the stress level and temperature were suitable to retain a significant amount of compressive stress in the sample, about 79 – 95% of the subsurface maximum RS in the baseline profile.

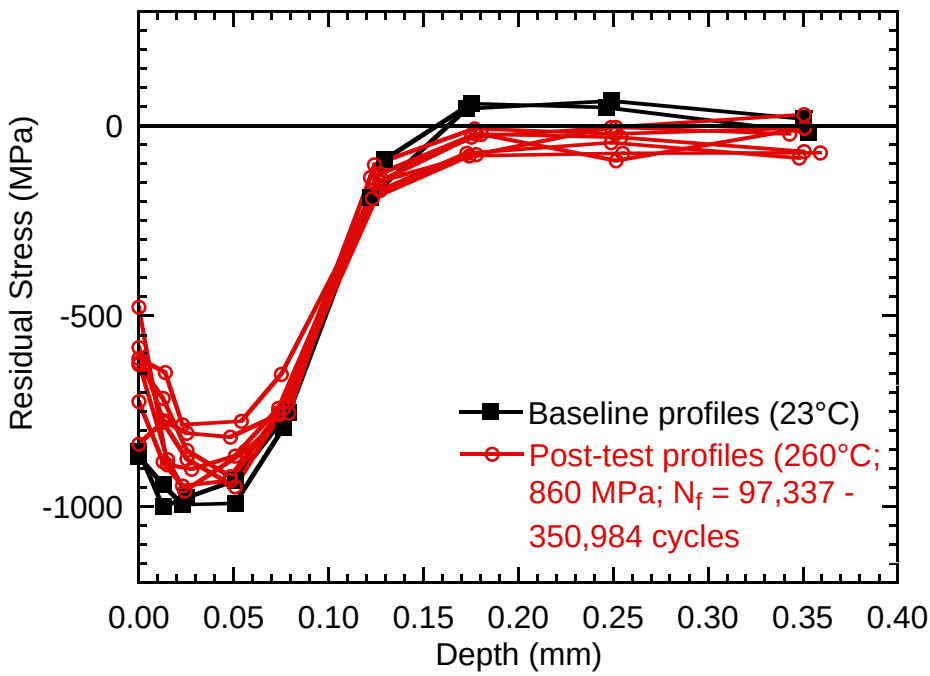

Fig. 4: Baseline and relaxed (post completion of test) RS profile in Ti-6-2-4-6.

4. RESULTS AND DISCUSSION

4.1 Fatigue variability behavior in the RS-free condition

The fatigue variability behavior of microstructures A and B at 260°C in the RS-free (i.e., electropolished) condition is presented in Fig. 5. A more detailed discussion in terms of the effect of microstructure and temperature on the lifetime variability has been provided in [27]. In the figure, the experimental points have been plotted on the Cumulative Distribution Function (CDF) scale, using the lognormal model. In both microstructures, a step-like behavior of data, as illustrated by the dashed lines, was observed. In Ti-6-2-4-6, this has been attributed to a superposition of the crack-growth-controlled (life-limiting) mechanism with the crack-initiation-dominated (mean) behavior [27]. The effect of microstructural and extrinsic variables on the lifetime variability can then be modeled in terms of the distinct influence of these on the crack

initiation and growth regimes, affecting the degree of separation between the two superimposing behaviors, as shown in [27-29].

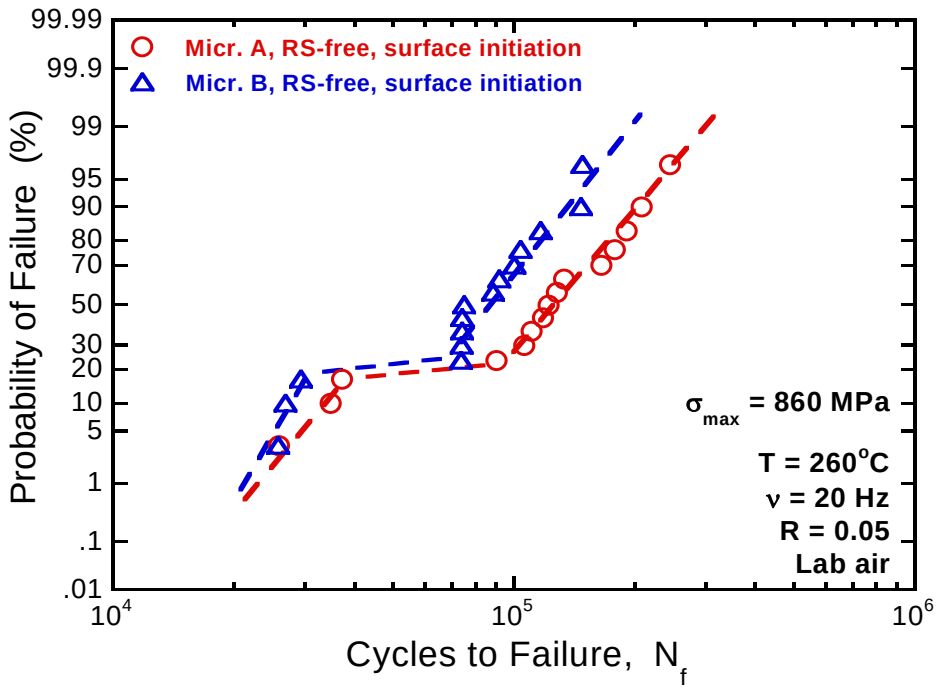

Fig. 5: Fatigue variability behavior in Ti-6-2-4-6 in the RS-free condition at 260°C.

Figure 5 also points to the very similar lower-tail of the lifetime distribution (the observed minimum lifetimes being 25,851 vs. 25,744 cycle in microstructures A and B respectively) in the two microstructures, which can be attributed to their very similar small and long crack growth behavior [27]. At the same time, the longer mean-lifetime (about 125,945 vs. 83,206 cycles respectively), as well as the increased lifetime variability in microstructure A was suggested to arise from a separation between the crack-initiation-controlled responses of the two [27, 29] due to a much greater sensitivity of the crack initiation regime to even a moderate degree of microstructural modification.

Failure mechanism in the RS-free case

In terms of the crack-initiation mechanism, in the RS-free condition (i.e., electropolished surface), failures occurred exclusively by surface-initiation, as indicated in Fig. 5. By surface initiation it is implied that crack initiating microstructural feature either intersected the surface or was within one primary-α diameter (about 4 μm) from the surface. A typical crack origin in the RS-free case in microstructure B is shown in Fig. 6. Quantitative details on the crack initiation features, in terms of their size and angle with respect to the loading axis, are provided in Section 4.3. As shown in Fig. 6 (a), crack initiation could characteristically be traced to facet formation in an equiaxed primary-α (α_p) particle, on the size scale of approximately 10 μm. In some cases, two or three adjacent α_p and/or colony-facets represented the surface crack initiation site. Measurements of the facet angle with respect to the loading axis revealed that the facet planes were oriented for shear or slip deformation. This is also evident in the tilted fractograph (30° with respect to the loading axis) in Fig. 6(b). In this, the facet-forming primary-α is indicated on the side surface of the sample and can be seen to contain parallel slip marks. The surface crack initiation under the RS-free condition can therefore, be considered as highly crystallographic in nature. In the same alloy, at 23°C and in the RS-free state, an increase in the incidence of subsurface-initiated failures was reported with a decrease in the stress level [32] but at 860 MPa, a majority of failures were by a surface-initiation mechanism. It is a reasonable supposition that in Ti-6-2-4-6, in the absence of surface RS, the surface crack-initiation in one or a few microstructural units will predominate, especially at an elevated temperature.

4.2 Effect of SP on the lifetime distribution

The SP treatment produces longer mean lifetimes, often by promoting subsurface crack initiation [7, 8]. This is particularly the case in smooth fatigue in the intermediate lifetime range, where in an otherwise RS-free condition failure would occur by surface crack-initiation [6, 15].

At stress levels, where significant mechanical relaxation of the RS is favored, failure by surface-initiation is generally reported [7, 12, 20, 21], in which the SP benefit to lifetime is nominally reduced. The emphasis in this study has been on the distribution in lifetime at an intermediate stress level where significant amount of RS is retained upon fatigue loading, and the dominant failure mechanism in the absence of RS is by surface crack initiation.

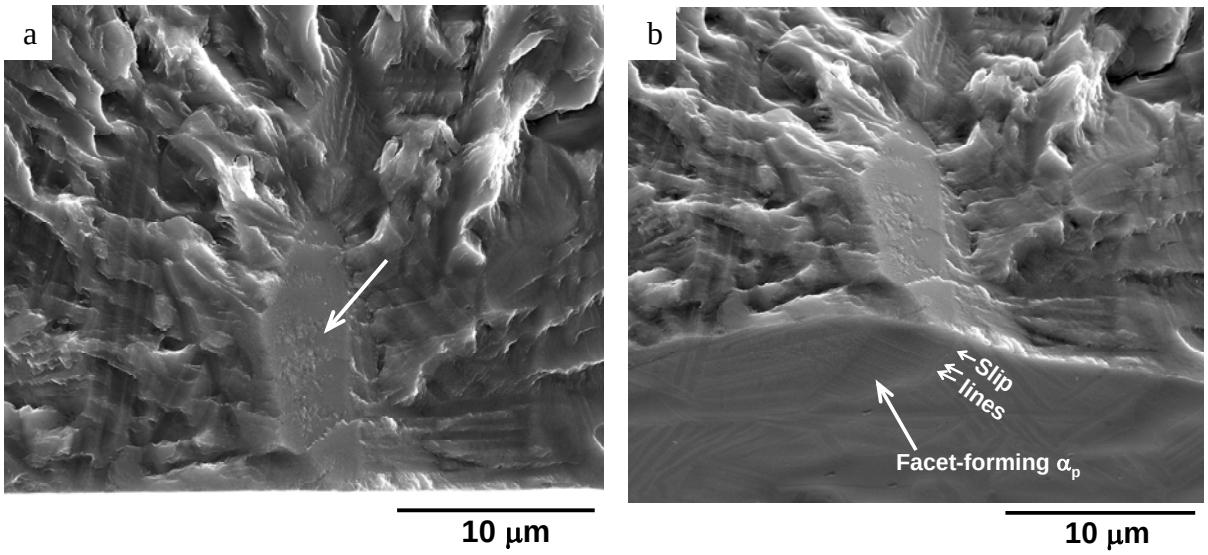

Fig. 6: Crack initiation characteristics in the RS-free condition at 260°C in microstructure B. Crack initiation facet shown at a tilt of (a) normal to the loading axis and (b) 30° with respect to the loading axis.

The lifetime distributions in microstructures A and B in the SP condition are compared to the RS-free state in Fig. 7. The surface and subsurface failures have been depicted by open and closed symbols respectively. Several key features of the fatigue variability behavior under SP are apparent from Fig. 7. First, there is a clear benefit of SP in terms of the mean-lifetime behavior. Second, unlike the RS-free condition, the lifetime distributions under SP display segregation in terms of surface and subsurface-initiated mechanisms. Third, a strong role of microstructure in the probability of surface versus subsurface-initiated failure is evident, in that in the given

number of experiments, crack initiation is driven to the subsurface in almost all experiments in microstructure A but less than 50% of the tests in microstructure B.

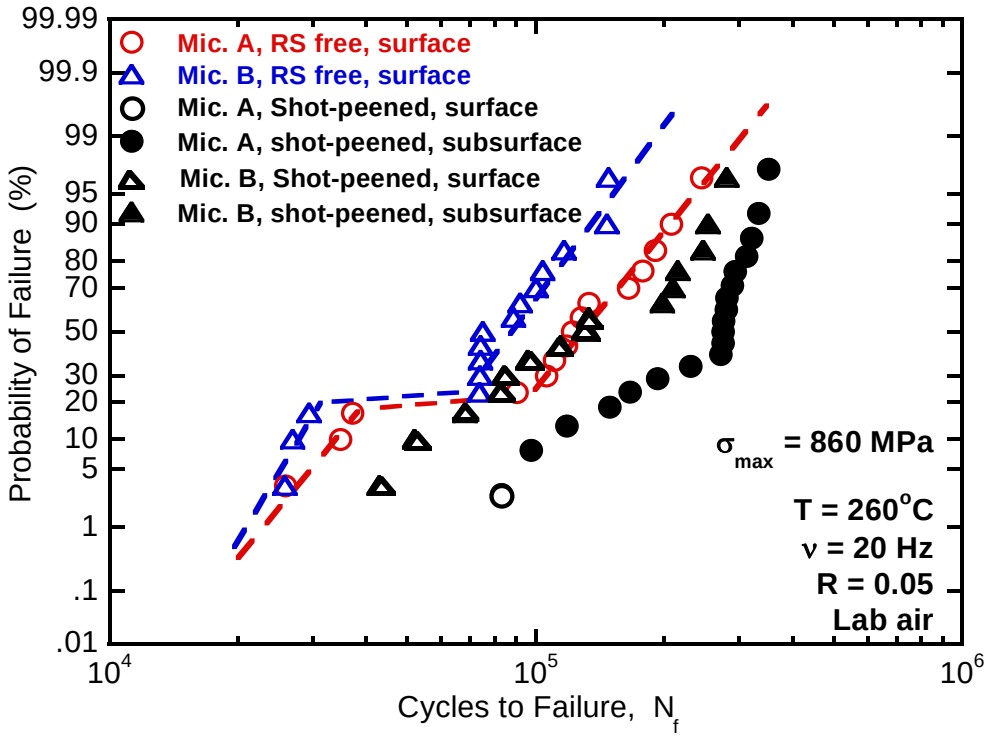

Fig. 7: Fatigue variability behavior in Ti-6-2-4-6 in the SP condition at 260°C.

Given the variability in the relaxed RS profile (Fig. 4), an important consideration is whether the degree of relaxation correlates with lifetime. The crack initiation distance from the surface is plotted against lifetime in Fig. 8 (a) and the compressive RS upon relaxation (surface and maximum subsurface RS which occurs at a depth just below the surface) is plotted in Fig. 8(b) for selected samples in which the RS profiles were obtained. The points in Fig. 8(b) represent only the subsurface-initiated failures. The average depth of compressive RS upon relaxation is demarcated by the shaded area in Fig. 8(a). Although the subsurface failures initiated beyond the compressive RS depth region, the center of crack initiation ranging from about 230 to 1748 μm from the surface, there is no clear relationship of the depth of initiation with lifetime. Furthermore, Fig. 8(b) indicates that the retained nominal profile does not correlate

with lifetime and in these samples subsurface initiation was favored across a wide range of values of the surface or the maximum compressive RS. This is not surprising, considering that in the absence of RS the surface crack initiation mechanism involves facet formation on the order of the equiaxed or lath α size, therefore, the retained RS levels being more than sufficient in mitigating this mechanism.

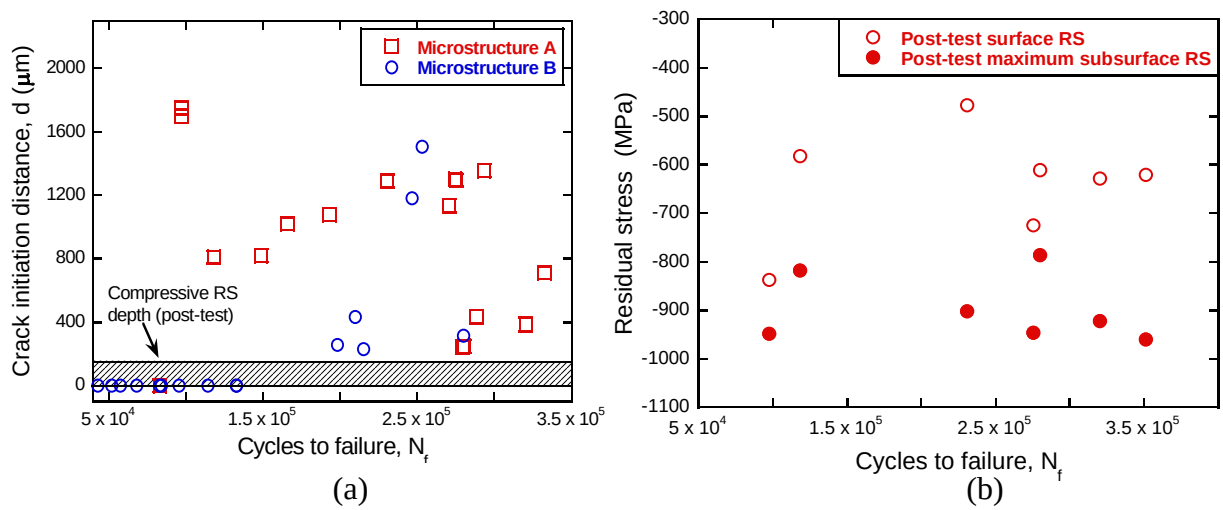

Fig. 8: Effect of the post-test RS level on the crack initiation distance from the surface and the lifetime; (a) Crack initiation distance versus lifetime and (b) Surface and maximum subsurface RS level as a function of lifetime.

An analysis of the effect of variability in the retained RS profile on the driving force for surface versus subsurface crack propagation will be presented in a forthcoming paper. Given that surface crack initiation in the RS-free state involves crystallographic-facet formation on the size scale of a primary-α particle (about 10 μm), in spite of the variability in the RS relaxation, it is reasonable to expect the failure-initiation to shift to the subsurface region especially when a significant amount of compressive RS is retained. In this regard, the subsurface failures in Fig. 7 can be considered as governed by the nominal RS profile. The surface failures, on the other hand, are suggested to arise due to more localized SP-material interaction events, as discussed in the following section. From a life-prediction perspective, this indicates that a probabilistic

description of the fatigue response that integrates the nominally-driven versus the locally-controlled effects may provide a platform for including appropriate credit of a surface treatment in life prediction.

4.3 Nominal vs. life-limiting failure mechanisms under SP

Typical crack initiation characteristics in the RS-free case, presented in Fig. 6, revealed facet formation in a surface α particle and/or α/β colony. As discussed above, under SP, the lifetime distribution separated into subsurface and surface-initiated failures. These two modes of crack initiation in microstructure B are shown in Figures 9 and 10 respectively. Microstructure A also displayed the same crack initiation characteristics. The size (in terms of the diameter of the circle, equivalent to the crack-initiation area) and the spatial angle of the crack-initiation feature with reference to the loading axis in representative samples of each microstructure are given in Fig. 11 (a) and (b) respectively. These figures illustrate the key contrasts between the nature of crack initiation under the RS-free and the SP condition, as discussed next.

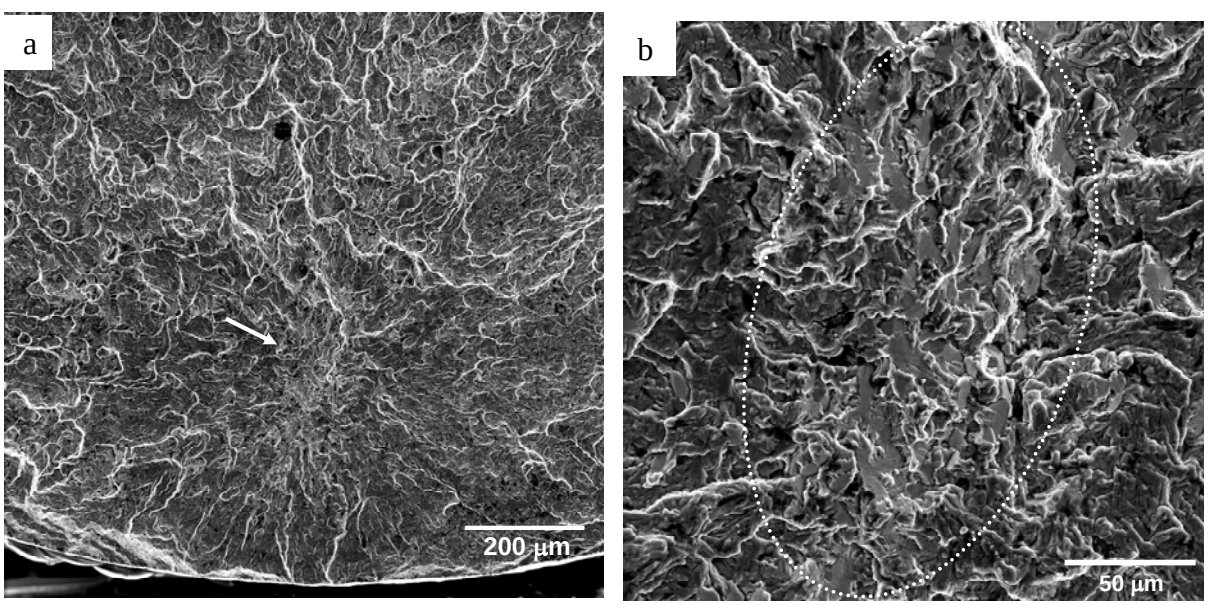

Fig. 9: Subsurface (center of crack initiation is about 315 μm from the surface) crack initiation under SP condition at 260°C; (a) an overview of the crack origin and (b) Crack initiation mechanism indicating a large field of α facet formation.

As noted previously, the shift to subsurface initiation is expected under SP due to the small surface crack initiation size in the absence of surface RS and is considered to be the response to the nominal RS profile. Figure 9(a) shows an overview of the subsurface initiation, where the center of crack initiation was approximately 315 μm from the surface, and indicates a significantly larger crack initiation area than in the RS-free case. In particular, in the RS-free condition, Figs. 6 and 11 show that crack initiated within single (or a few contiguous) microstructural unit (about 10 μm in equivalent diameter) by facet formation along a crystallographic plane that is at an angle of about 30 - 45° with respect to the loading axis (Fig. 11(b)). The subsurface initiation under SP also occurred by crystallographic faceting (Fig. 9(b)) such that the facet angles were approximately 30 – 50° with respect to the loading axis (Fig. 11(b)) but in a collection of equiaxed and lath α, spread over a much larger area with the equivalent diameter of about 100 - 200 μm (Fig. 11(a)). To be noted, that the crack initiation size for subsurface initiation, plotted in Fig. 11(a), was taken as the diameter of the circle equivalent to the polygon circumscribing the field of faceting at the crack origin. Multiple points at a given lifetime of a subsurface-initiated failure in Fig. 11(b) represent the collection of facets forming a given crack initiation area.

The surface crack initiation mechanism under SP is presented in Fig. 10 and appears to have occurred by a large scale non-crystallographic fracture, in that the fracture was indiscriminating with respect to microstructural phases or crystallographic planes, Fig. 10(a). A switch in the fracture topology, from nearly flat fracture morphology at the crack initiation site to the classical crack growth type morphology was observed, as approximately demarcated in Fig. 10(a). Figure 10(b) shows the inverted version of the image in Fig. 10(a), in which the average topographic differences between the crack initiation area and the crack growth region are more easily

visualized. This is further illustrated with the help of the digital elevation map (DEM) of the crack initiation region, Fig. 10(c). The DEM was constructed by the quantitative tilt fractography technique employing the MeX 3D image analysis program. In Fig. 10(c), the DEM has been rotated counterclockwise by about 60° and 30° respectively with reference to the X and Y axis in the configuration shown in Figs. 10(a) and (b) in order to provide a clearer visualization of the fracture features and the transition between the two types of morphologies. The ends of the crack

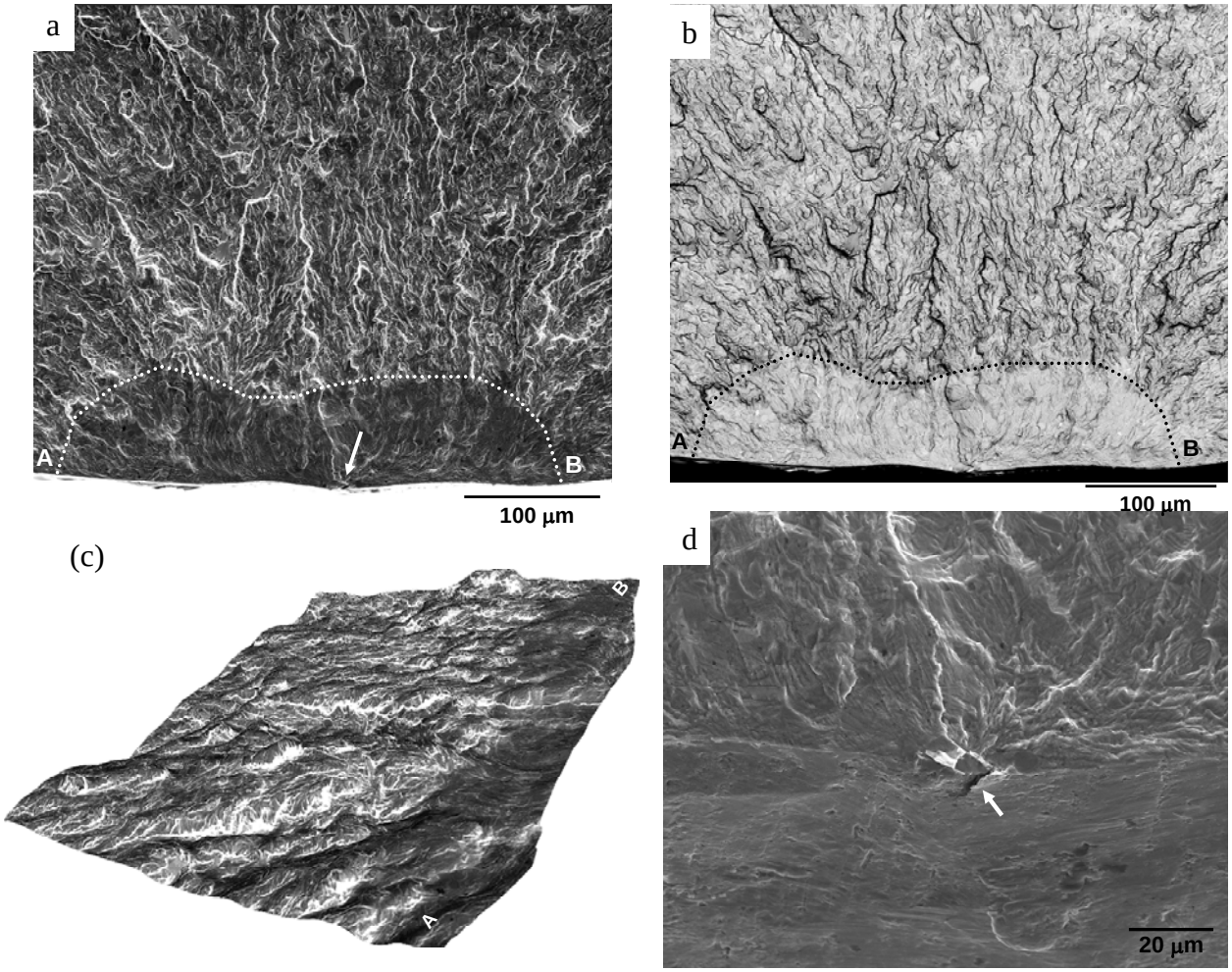

Fig. 9: Surface crack initiation mechanism under SP condition in microstructure B; (a) surface initiation site indicating a large non-crystallographic fracture area, (b) A version of the image in (a) where the colors have been inverted, (c) the digital elevation map of the crack initiation region revealing the transition between the flat fracture morphology and ductile crack growth, and (d) Detailed view of the notch-like surface feature, where the sample is shown at a tilt of 45° with respect to the loading axis

initiation site have been indicated in Figs. 10(a), (b), and (c). The transition between the flat-fracture area and the metallic-crack-growth-type morphology is clearly apparent in Fig. 10(c). As shown, the shape of this area was invariably shallower in the depth direction than along the surface. The second key characteristic of the surface crack origin, evident in most cases, was that crack initiation was associated with a (or more) sharp roughness feature, indicated in Fig. 10(a) and shown in detail in Fig. 10(d). In Fig. 10(d), the sample is shown at a tilt of 45° with respect to the loading axis. The size of the non-crystallographic area was measured in representative samples and is plotted in Fig. 11(a) in terms of the equivalent diameter, which was roughly between 60 and 200 μm. Further, Fig. 11(b) depicts that the flat-fracture area was close to the normal to the loading axis.

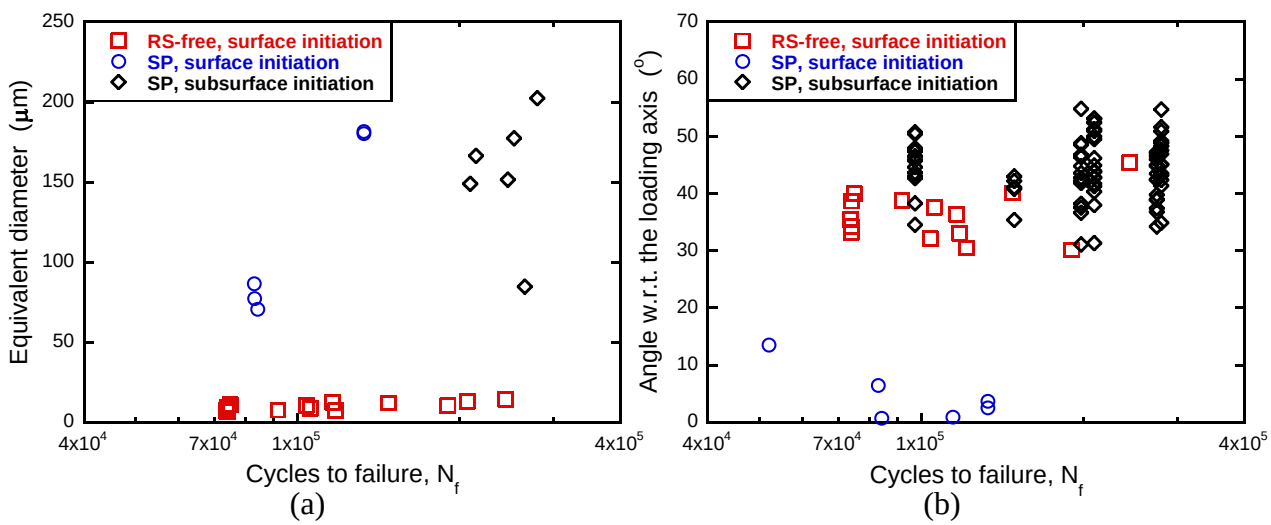

Fig. 10: Crack initiation characteristics under RS-free and SP conditions in Ti-6-2-4-6; (a) crack initiation size in terms of the equivalent diameter and (b) angle of fracture plane with respect to the loading axis.

Although near-normal to the loading axis, given the radial crack growth patterns (Fig. 10(a)), it appears that the flat region found in surface initiation sites may not have developed by instantaneous fracture across the entire area. While the surface layer has a nominal work

hardening level, locally the degree of hardening may fluctuate depending on the underlying microstructure. One possible mechanism of formation of the large non-crystallographic fracture area can be via rapid fatigue crack initiation and growth in a critically work-hardened location coincident with a notch-like roughness feature. The longer surface length than the depth of the flat region may also signify a rapid formation of this area, as opposed to by slow crack growth, in which the crack is generally found to grow significantly faster in the depth direction due to the RS gradient [10]. The surface crack initiation size under SP, plotted in Fig. 11(a), pertains to this hypothesis and has been speculated to be effectively equivalent to the non-crystallographic, flat fracture area. However, as evident from Fig. 10, due to the uncertainty in precisely determining the boundary between the non-crystallographic area and the ductile crack-growth morphology, the surface crack initiation sizes under SP in Fig. 11(a) should be considered as approximate.

Given the above analysis of the competing nominal vs. local effects of SP and associated crack initiation sizes and mechanisms, it can be emphasized that the nominal RS profile eliminates the crystallographic, microstructure-scale surface crack initiation mechanism in favor of a much larger scale crystallographic initiation from the subsurface. However, coexistent with this nominal-RS-driven behavior is another surface-initiated mechanism, attributed to randomly occurring localized surface events, by non-crystallographic crack initiation and significantly larger crack initiation size than in the RS-free case. Here it is useful to note the peening configuration in terms of the shot size relative to the size and the geometry of the specimen. This is illustrated by Fig. 3 where relative dimensions are to the scale. Considering that spherical shots of diameter 0.5 mm were employed on a cylindrical specimen of about 4 mm diameter the local SP-affected regions may, partly be contributed by the nature of contact between the shots and the specimen.

4.4 Accounting for a surface treatment in life Prediction

This study shows that it may be useful in life-prediction to consider a mean versus life-limiting description of fatigue variability, in which the two behaviors respond differently to microstructure and extrinsic variables. Therefore, the effect of a surface treatment, such as SP, on a material has to be assessed both in terms of the influence on its mean-lifetime but more importantly the impact on the lower-tail of the lifetime distribution, which is controlled by factors very distinct from those governing the mean response and pursues different crack initiation mechanism and size. For instance, in this approach, the effect of increased peening intensity on fatigue lifetime can be represented in terms of the separation of the effects of higher nominal RS level, and the localized SP-process-induced factors. Thereby, while the former effect may increase the nominal lifetime, the latter might in fact increase the propensity for life-limiting, surface-initiated failures due to increased possibility of localized work-hardened regions and surface notch-like features. Such lifetime trends with respect to the peening intensity have been reported by other researchers [7], where a high SP intensity was shown to favor surface-initiated failures in rotating-bending fatigue while an intermediate intensity produced the maximum benefit on lifetime by promoting subsurface failures in majority of the samples (at lower stress levels).

Besides the separation into the two distributions, another key aspect in life-prediction or the assessment of the effect of SP on lifetime, evident from this paper, is that the surface crack initiation size is different for the RS-free and the SP cases. This needs to be accounted for in an accurate prediction of the lower-tail of the lifetime distribution under the SP treatment.

Finally, it is to be noted, that the inherent lower-tail-lifetime (or the life-limiting distribution) response being emphasized here is expected to arise in spite of an otherwise

nominally perfect surface-treatment. This is to draw a distinction with homogeneous extrinsic factors such as lack of perfect coverage and over-aggressive treatment, which have been reported by several researchers [33 - 34] to affect the average fatigue behavior. It is recognized, however, that these extrinsic effects may randomly occur in any surface and will compliment the localized microstructural effects in driving the lower-tail of lifetime.

5. SUMMARY

To summarize, this paper demonstrates that the effect of a surface treatment such as SP on fatigue lifetime variability needs to be accounted in terms of the nominal vs. the local effects. In the present problem, the nominal RS levels induced by SP is found to drive the failure to the subsurface region, producing substantial lifetime benefits with reference to the RS-free case. However, the subsurface failure distribution was accompanied by the life-limiting distribution that was controlled by the local, SP-material interaction events, irrespective of the amount of retained nominal RS level, and these failures approached the lifetimes under the RS-free condition. This nominal vs. local effect was found to be strongly dependent on the microstructure, a further indication of the influence of local microstructure in producing the life-limiting crack initiation mechanism.

Acknowledgements

This work was performed at the Air Force Research Laboratory, Materials and Manufacturing Directorate, Wright-Patterson Air Force Base, OH. The financial support of the Air Force Office of Scientific Research (AFOSR) through the AFOSR task no. 92ML02COR with Dr. Victor Giurgiutiu as the program manager is gratefully acknowledged. We are also grateful for the

partial financial support of the Defense Advanced Research Project Agency (DARPA) under DARPA orders M978, Q588, P699, and S271 with Dr. Leo Christodoulou as the program manager. We also acknowledge Dr. Dennis Buchanan for the very helpful discussions and for his assistance with residual stress measurements.

References

[1] L. Wagner, Ed., *Shot Peening*, Wiley-VCH, 2002.

[2] A. Drechsler, T. Dorr, and L. Wagner, "Mechanical surface treatments on Ti-10-2-3 for improved fatigue resistance," *Mater Sci Engng*, Vol. A243, pp. 217-220, 1998.

[3] J. D. Almer, J. B. Cohen, and B. Moran, "The effect of residual macrostresses and microstresses on fatigue crack initiation," *Mater Sci Engng*, Vol. A284, pp. 268-279, 2000.

[4] E. R. De Los Rios, A. Walley, M. T. Milan, and G. Hammersley, "Fatigue Crack Initiation and Propagation on Shot Peened Surfaces in A316 Stainless Steel," *Int J Fatigue*, Vol. 17, pp. 493-499, 1995.

[5] R. K. Nalla, I. Altenberger, U. Noster, G. Y. Liu, B. Scholtes, and R. O. Ritchie, "On the influence of mechanical surface treatments – deep rolling and laser shock peening - on the fatigue behavior of Ti-6Al-4V at ambient and elevated temperatures," *Mater Sci Engng*, Vol. A355, pp. 216-230, 2003.

[6] G. S. Was and R. M. Pelloux, "The Effect of Shot Peening on the Fatigue Behavior of Alloy 7075-T6," *Metallurgical Trans. A*, Vol. 10A, pp. 656-658, 1979.

[7] M. A. S. Torres and H. J. C. Voorwald, "An evaluation of the shot-peening residual stress and stress relaxation on the fatigue life of AISI 4340 steel," *Int J Fatigue*, Vol. 24, pp. 877-886, 2002.

[8] J. Lindeman, C. Buque, and F. Appel, "Effect of shot-peening on fatigue performance of a lamellar titanium aluminide alloy," *Acta Materialia*, Vol. 54, pp. 1155-1164, 2006.

[9] R. John, J. M. Larsen, D. J. Buchanan, and N. E. Ashbaugh, "Incorporating Residual Stresses in Life Prediction of Turbine Disks," NATO RTO (AVT) Symposium on Monitoring and Management of Gas Turbine Fleets for Extended Life and Reduced Costs, Oct 8-11, 2001.

[10] M. Beghini, L. Bertini, and E. Vitale, "Fatigue crack growth in residual stress fields," *Fatigue Fract Engng Mater Structures*, Vol. 17, pp. 1433-1444, 1994.

[11] C. H. Wang, S. A. Barter, and Q. Liu, "A closure model to crack growth under large scale yielding and through residual stress fields," *J Engng Mater Tech*, Vol. 125, pp. 183-190, 2003.

[12] G. A. Webster and A. N. Ezeilo, "Residual stress distributions and their influence on fatigue lifetimes," *Int J Fatigue*, Vol. 23, pp. S375-S383, 2001.

[13] E. Hornbogen, M. Thumann, and C. Verpoort, "Influence of Shot Peening on the Fatigue Behavior of a Precipitate Hardenable Austenitic Steel," *Proc. Ist International Conference on Shot Peening*, ICSP 1, Pergamon Press, Oxford, pp. 381-387, 1987.

[14] A. Turnbull, E. R. De Los Rios, R. B. Tait, C. Laurant, and J. S. Boabaid, "Improving the Fatigue Resistance of Waspaloy by Shot Peening," *Fatigue Fract Engng Mater Struct*, Vol.21, pp. 1513-1524, 1998.

[15] R. C. McClung, "A literature survey on the stability and significance of residual stresses during fatigue," *Fatigue Fract Engng Mater Struct*, 30, 173-205.

[16] Y. Mutoh, G. H. Fair, B. Noble, and R. B. Waterhouse, "The Effect of Residual Stresses Induced by Shot-Peening on Fatigue Crack Propagation in Two High Strength Aluminum Alloys," *Fatigue Fract Engng Mater Struct*, Vol. 10, pp. 261-272, 1987.

[17] E. R. De Los Rios, M. Trull, and A. Levers, "Modelling Fatigue Crack Growth in Shot-Peened Components of Al 2024-T351," *Fatigue Fract Engng Mater Struct*, Vol. 23, pp. 709-716, 2000.

[18] C. A. Rodopoulous, S. A. Curtis, E. R. De Los Rios, and J. Solisromero, "Optimization of the fatigue resistance of 2024-T351 aluminum alloys by controlled shot-peening methodology," *Int J Fatigue*, Vol. 26, pp. 849-856, 2004.

[19] Z. L. Lu, S. X. Li, Y. Y. Lui, Q. Y. Zhang, J. F. Lei, and Z. X. Mu, "Effects of surface treatments on fatigue life of Ti-6-22-22 alloy at room and high temperatures," *Mater Sci Engng*, Vol. A383, pp. 283-288, 2004.

[20] M. C. Berger and J. K. Gregory, "Residual stress relaxation in shot peened Timetal 21S," *Mater Sci Engng*, Vol. A263, pp. 200-204, 1999.

[21] W. Z. Zhuang and G. R. Halford, "Investigations of residual stress relaxation under cyclic load," *Int J Fatigue*, Vol. 23, pp. S31-S37, 2001.

[22] B. L. Boyce, X. Chen, J. O. Peters, J. W. Hutchinson, and R. O. Ritchie, "Mechanical relaxation of localized residual stresses associated with foreign object damage," *Mater Sci Engng*, Vol. A349, pp. 48-58, 2003.

[23] D. J. Buchanan and R. John, "Relaxation of Shot-Peened Residual Stresses under Creep Loading," *Scripta Materialia*, Vol. 59, pp. 286-289, 2008.

[24] R. John, D. J. Buchanan, S. K. Jha, and J. M. Larsen, "Stability of Residual Stresses in Shot-Peened Ti-6Al-2Sn-4Zr-6Mo," to be published, 2008.

[25] S. Curtis, E. R. de Los Rios, C. A. Rodopoulos, and A. Levers, *Int. J. Fatigue*, Vol. 25, pp. 59-66, 2003.

[26] G. R. Leverant, B. S. Langer, A. Yuen, and S. W. Hopkins, "Surface Residual Stresses, Surface Topography and the Fatigue Behavior of Ti-6Al-4V," *Metallurgical Trans. A*, Vol. 10A, pp. 251-257, 1979.

[27] S. K. Jha, M. J. Caton, and J. M. Larsen, "A New Paradigm of Fatigue Variability Behavior and Implications for Life Prediction," *Mater Sci Engng A*, 2007.

[28] S. K. Jha, M. J. Caton, and J. M. Larsen, "Mean vs. Life-Limiting Fatigue Behavior in a Nickel-Based Superalloy," In Press, *Superalloys-2008*, 2008.

[29] S. K. Jha and J. M. Larsen, *VHCF-4*, 2007.

[30] C. J. Szczepanski, S. K. Jha, J. M. Larsen, and J. W. Jones, In Press, *Metallurgical and Materials Transactions A*, 2008.

[31] P. S. Prevey, "Current Applications of X-ray Diffraction Residual Stress Measurement," *Developments in Materials Characterization Technologies*, C. Vander Voort and J. Friel, Eds., ASM International, Materials Park, OH, pp. 103-110, 1996.

[32] S. K. Jha, J. M. Larsen, A. H. Rosenberger, and G. A. Hartman, *Scripta Materialia*, 2003.

[33] L. Wagner and G. Lutjering, "Influence of the Shot Peening Parameters on the Surface Layer Properties and the Fatigue Life of Ti-6Al-4V," *Proceedings of ICSP-2*, pp. 194-200, 1984.

[34] J. T. Cammett, P. S. Prevey, and N. Jayaraman, "The Effect of Shot Peening Coverage on Residual Stress, Cold Work, and Fatigue in Ni Base Superalloy," *Proceedings of ICSP-9*, 2005.